

RESEARCH ARTICLE | MARCH 08 2024

Rationale for the extrapolation procedure in selected configuration interaction

Hugh G. A. Burton  ; Pierre-François Loos 



J. Chem. Phys. 160, 104102 (2024)

<https://doi.org/10.1063/5.0192458>



View
Online



Export
Citation

CrossMark

Boost Your Optics and Photonics Measurements

Lock-in Amplifier

Zurich Instruments

Find out more

Boxcar Averager

Rationale for the extrapolation procedure in selected configuration interaction

Cite as: J. Chem. Phys. 160, 104102 (2024); doi: 10.1063/5.0192458

Submitted: 19 December 2023 • Accepted: 18 February 2024 •

Published Online: 8 March 2024



View Online



Export Citation



CrossMark

Hugh G. A. Burton^{1,a)} and Pierre-François Loos^{2,b)}

AFFILIATIONS

¹ Yusuf Hamied Department of Chemistry, University of Cambridge, Lensfield Road, Cambridge CB2 1EW, United Kingdom

² Laboratoire de Chimie et Physique Quantiques (UMR 5626), Université de Toulouse, CNRS, UPS, Toulouse, France

Note: This paper is part of the 2024 JCP Emerging Investigators Special Collection.

a) Author to whom correspondence should be addressed: hgaburton@gmail.com

b) Electronic mail: loos@irsamc.ups-tlse.fr

ABSTRACT

Selected configuration interaction (SCI) methods have emerged as state-of-the-art methodologies for achieving high accuracy and generating benchmark reference data for ground and excited states in small molecular systems. However, their precision relies heavily on extrapolation procedures to produce a final estimate of the exact result. Using the structure of the exact electronic energy landscape, we provide a rationale for the common linear extrapolation of the variational energy as a function of the second-order perturbative correction. In particular, we demonstrate that the energy gap and the coupling between the so-called internal and external spaces are the key factors determining the rate at which the linear regime is reached. Starting from the first principles, we also derive a new non-linear extrapolation formula that improves the post-processing of data generated from SCI methods and can be applied to both ground- and excited-state energies.

© 2024 Author(s). All article content, except where otherwise noted, is licensed under a Creative Commons Attribution (CC BY) license (<http://creativecommons.org/licenses/by/4.0/>). <https://doi.org/10.1063/5.0192458>

I. INTRODUCTION

Selected configuration interaction (SCI)^{1–4} and related methods (such as density-matrix renormalization group approaches^{5–7} and others^{8–17}) have taken a prominent role in modern electronic structure theory.^{18–20} Their primary purpose is to calculate reference correlation and excitation energies in small molecular systems,^{19,21–28} for which they have demonstrated a remarkable ability to yield highly accurate estimates of full configuration interaction (FCI) results. The numerous variations of SCI all perform a sparse exploration of the Hilbert space by selecting only the most energetically relevant determinants. This natural philosophy emerges from the observation that, among the incredibly large number of determinants in the FCI space, only a tiny fraction of them significantly contribute to the energy. Modern versions of SCI include CIPSI (CI using a Perturbative Selection made Iteratively),^{3,18,21,29–36} adaptive sampling CI (ASCI),^{37–40} semi-stochastic heatbath CI (SHCI),^{23,24,41–45} and iterative CI (iCI).^{46–50} Stochastic CI methods, such as Monte Carlo CI (MCCI)^{51,52} and FCI quantum Monte Carlo (FCIQMC),^{53–58} follow a similar

philosophy by using a stochastic representation to select the most important determinants.

The SCI wave function corresponds to a truncated CI expansion constructed from determinants in some internal (or model) space \mathcal{I} ,

$$|\Psi_{\text{var}}\rangle = \sum_{I \in \mathcal{I}} c_I |I\rangle, \quad (1)$$

with the associated variational energy $E_{\text{var}} = \langle \Psi_{\text{var}} | \hat{H} | \Psi_{\text{var}} \rangle$, where we assume the normalization of the variational wave function, i.e., $\langle \Psi_{\text{var}} | \Psi_{\text{var}} \rangle = 1$. The accuracy of $|\Psi_{\text{var}}\rangle$ can be assessed using the second-order Epstein–Nesbet perturbation correction, computed using the determinants $\{\alpha\}$ that lie outside the model space (i.e., in the external space \mathcal{A}) as

$$E_{\text{PT2}} = - \sum_{\alpha \in \mathcal{A}} \frac{|\langle \Psi_{\text{var}} | \hat{H} | \alpha \rangle|^2}{H_{\alpha\alpha} - E_{\text{var}}}, \quad (2)$$

where $H_{\alpha\alpha} = \langle \alpha | \hat{H} | \alpha \rangle$. This perturbative approximation is traditionally derived using Löwdin partitioning, as shown in Appendix A.

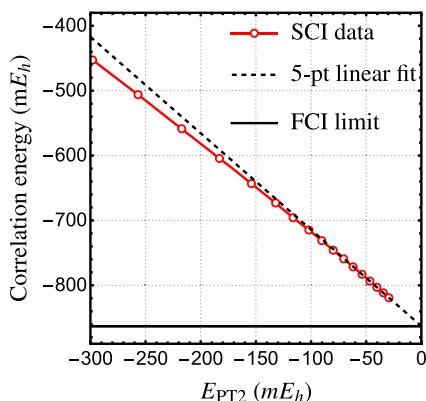


FIG. 1. Frozen-core (variational) correlation energy of benzene as a function of E_{PT2} computed on the cc-pVDZ basis, as described in Ref. 35.

The exact FCI wave function and energy are indicated by the limit $E_{\text{PT2}} \rightarrow 0^-$.

Despite the sparse exploration of the Hilbert space, these state-of-the-art methods still rely heavily on extrapolation procedures to produce final FCI estimates.^{19,20,23,34} In particular, it is widely observed that an approximate linear relationship appears between E_{var} and E_{PT2} when E_{PT2} becomes small enough, and thus, a linear or quadratic extrapolation of E_{var} for $E_{\text{PT2}} \rightarrow 0$ is generally used to estimate the exact energy for an unconverged SCI calculation.²³ The precision and reliability of this post-processing extrapolation procedure are critical in order to produce meaningful estimates. However, to the best of our knowledge, no theoretical justification for the linear (or otherwise) relationship between E_{var} and E_{PT2} has been proposed.

To illustrate this extrapolation procedure, Fig. 1 shows the evolution of the variational correlation energy of benzene as a function of E_{PT2} , computed with the cc-pVDZ basis and within the frozen-core approximation. These SCI calculations were performed with the QUANTUM PACKAGE software using the CIPSI algorithm,³⁴ and the data are extracted from Ref. 35. The FCI estimate of the correlation energy (solid black line in Fig. 1) was estimated to be -862.890 mE_h and was obtained by performing a five-point linear fit (dashed black line in Fig. 1) of the CIPSI data. This estimate carries an error of the order of 1 mE_h , and the fitting error was estimated to be 0.266 mE_h . In Fig. 1, it is clear that, for sufficiently small E_{PT2} , the variational quantity is linear with respect to E_{PT2} . However, the SCI data deviate significantly from linearity for larger values of E_{PT2} , which we shall address in detail later on.

In this article, we provide a rationale to justify the linear extrapolation of the (zeroth-order) variational energy as a function of the second-order perturbative energy. We adopt a geometric approach that considers the variational wave function as a point on the exact electronic energy landscape,⁵⁹ allowing the second-order perturbative correction to be derived from the local gradient and curvature of this energy landscape. Moreover, we investigate a two-state model in which an analytic relationship between E_{var} and E_{PT2} can be derived, leading to a novel parameterized non-linear formula that facilitates a more robust extrapolation procedure.

II. RATIONALE FOR THE LINEAR EXTRAPOLATION

The linear relationship between E_{var} and E_{PT2} can be derived from the first principles by considering the structure of the electronic energy landscape. While Ref. 59 describes this energy landscape perspective in detail, the salient points are summarized here. Any normalized wave function in the full N -dimensional Hilbert space,

$$|\Psi\rangle = \sum_{I=1}^N v_I |I\rangle, \quad (3)$$

can be represented by a vector \mathbf{v} subject to the normalization constraint $\mathbf{v}^\dagger \cdot \mathbf{v} = 1$, which constrains the wave function to the surface of a hypersphere. The energy is given by the quadratic form,

$$E = \mathbf{v}^\dagger \cdot \mathbf{H} \cdot \mathbf{v}, \quad (4)$$

and exact eigenstates of the Hamiltonian correspond to stationary points of E constrained to the surface of the hypersphere, as illustrated in Fig. 2. At any point on the hypersphere, the tangent space \mathcal{T} contains the vectors that are orthogonal to \mathbf{v} , which can be collected as the columns of an $N \times (N - 1)$ matrix \mathbf{v}_\perp . These tangent vectors correspond to the states $|T\rangle$ that are orthogonal to $|\Psi\rangle$ and satisfy

$$\hat{1} = |\Psi\rangle\langle\Psi| + \sum_{T \in \mathcal{T}} |T\rangle\langle T|, \quad (5)$$

where $\hat{1}$ is the identity operator. A constrained step \mathbf{s} on this landscape is parameterized using a unitary transformation as

$$|\Psi(\mathbf{s})\rangle = \exp\left(\sum_{T \in \mathcal{T}} s_T (|T\rangle\langle\Psi| - |\Psi\rangle\langle T|)\right) |\Psi\rangle. \quad (6)$$

Assuming real wave functions, the components of the constrained energy gradient are then

$$g_T = \frac{\partial E}{\partial s_T} \Big|_{\mathbf{s}=0} = 2\langle T|\hat{H}|\Psi\rangle, \quad (7)$$

while the elements of the Hessian matrix of constrained second-derivatives become

$$Q_{TT'} = \frac{\partial^2 E}{\partial s_T \partial s_{T'}} \Big|_{\mathbf{s}=0} = 2\langle T|\hat{H} - E\hat{1}|T'\rangle. \quad (8)$$

So far, we have only considered the structure of the electronic energy landscape for an arbitrary wave function in the full Hilbert space. For a SCI variational wave function, the only non-zero elements of \mathbf{v} correspond to determinants included in the internal space, with coefficients c_I , as defined in Eq. (1). The tangent vectors can then be split into two disjoint sets corresponding to the eigenstates within the internal space that are orthogonal to $|\Psi_{\text{var}}\rangle$, denoted $\mathcal{J} = \{|J\rangle\}_{J \neq \text{var}}$, and the determinants in the external space, giving $\mathcal{T} = \mathcal{J} \cup \mathcal{A}$, as illustrated in Fig. 3. This separation of the internal and external spaces is further explained in Appendix A. Since $|\Psi_{\text{var}}\rangle$ is a CI solution within the internal space, such that $\langle J|\hat{H}|\Psi_{\text{var}}\rangle = 0$, the gradient in Eq. (7) is only non-zero in the direction of the tangent vectors in \mathcal{A} .

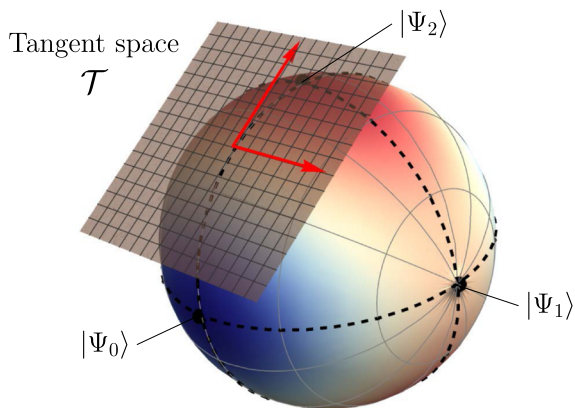


FIG. 2. Sketch of the exact electronic energy landscape in a three-dimensional Hilbert space. Eigenstates correspond to stationary points constrained to the surface of the unit sphere. At any point, the tangent space \mathcal{T} is spanned by the two vectors (red) that are orthogonal to the position vector.

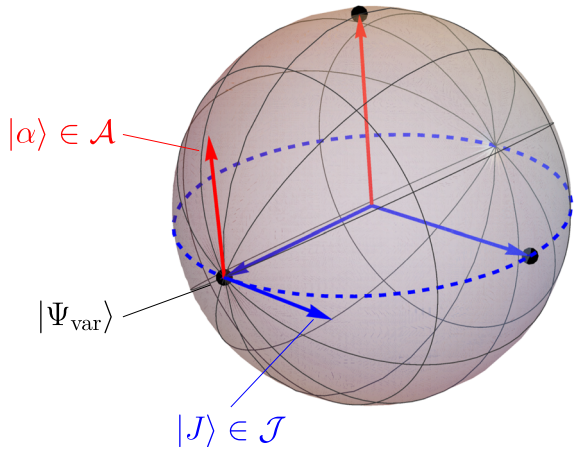


FIG. 3. Sketch of the tangent space construction $\mathcal{T} = \mathcal{J} \cup \mathcal{A}$. The variational space \mathcal{J} (dashed blue circle) is built from two configurations (blue vectors), and the external space \mathcal{A} contains one configuration (red vector). At $|\Psi_{\text{var}}\rangle$, the tangent space is spanned by one tangent direction $|J\rangle$, which is locally parallel to the variational space \mathcal{J} , and one orthogonal tangent direction in the external space $|\alpha\rangle$.

The local structure of the energy landscape around the variational wave function $|\Psi_{\text{var}}\rangle$ is given by a second-order Taylor series expansion as

$$E(\mathbf{s}) = E_{\text{var}} + \mathbf{s}^\dagger \cdot \mathbf{g} + \frac{1}{2} \mathbf{s}^\dagger \cdot \mathbf{Q} \cdot \mathbf{s}. \quad (9)$$

Optimizing this quadratic form with the Newton–Raphson step $\mathbf{s} = -\mathbf{Q}^{-1} \cdot \mathbf{g}$ gives an estimate of the difference between the exact energy E_{exact} and E_{var} as

$$\Delta E = E_{\text{exact}} - E_{\text{var}} \approx -\frac{1}{2} \mathbf{g}^\dagger \cdot \mathbf{Q}^{-1} \cdot \mathbf{g}, \quad (10)$$

or, equivalently,

$$\Delta E \approx - \sum_{\alpha \alpha' \in \mathcal{A}} \langle \Psi | \hat{H} | \alpha \rangle \langle \alpha | (\hat{H} - E_{\text{var}} \hat{1})^{-1} | \alpha' \rangle \langle \alpha' | \hat{H} | \Psi \rangle, \quad (11)$$

where we have exploited the fact that the gradient is zero in the direction of the tangent vectors within \mathcal{J} . Crucially, the exact energy landscape becomes quadratic near an eigenstate.⁵⁹ Therefore, Eq. (10) becomes an exact relationship when $|\Psi_{\text{var}}\rangle$ is sufficiently accurate, and we rigorously recover the linear asymptotic relationship,

$$E_{\text{var}} \sim E_{\text{exact}} - \Delta E \quad (\text{as } \Delta E \rightarrow 0). \quad (12)$$

The steps that we have taken to derive this asymptotic relation are analytically rigorous. However, the matrix elements $\langle \alpha | (\hat{H} - E_{\text{var}} \hat{1})^{-1} | \alpha' \rangle$ in Eq. (11) are too expensive to compute in practice. Instead, we can assume that the Hamiltonian is diagonally dominant in \mathcal{A} and take the leading order approximation,

$$\hat{H}^{(0)} = \sum_{II' \in \mathcal{I}} |I\rangle H_{II'} \langle I'| + \sum_{\alpha \in \mathcal{A}} |\alpha\rangle H_{\alpha\alpha} \langle \alpha|, \quad (13)$$

where $\hat{H}^{(0)}$ is the zeroth-order Hamiltonian within the Epstein–Nesbet partitioning. The energy correction then reduces to the second-order Epstein–Nesbet expression obtained in Eq. (2) to give

$$\Delta E \approx - \sum_{\alpha \in \mathcal{A}} \frac{|\langle \Psi_{\text{var}} | \hat{H} | \alpha \rangle|^2}{H_{\alpha\alpha} - E_{\text{var}}} = E_{\text{PT2}}. \quad (14)$$

Since E_{PT2} is the leading-order approximation to ΔE , we obtain $\Delta E \sim E_{\text{PT2}}$ for $\Delta E \rightarrow 0$. Therefore, when $|\Psi\rangle$ is sufficiently close to an eigenstate, we obtain the asymptotic relationship,

$$E_{\text{var}} \sim E_{\text{exact}} - E_{\text{PT2}} \quad (\text{as } E_{\text{PT2}} \rightarrow 0), \quad (15)$$

which justifies a linear extrapolation of E_{var} against E_{PT2} .

The only approximation employed in our derivation is to assume that Eq. (14) provides the dominant contribution to Eq. (11). From the exact energy landscape, we have shown that the asymptotic behavior of E_{var} is linear for any SCI variational wave function as $E_{\text{PT2}} \rightarrow 0$ and that the slope of this relationship is close to -1 for $E_{\text{var}} \rightarrow E_{\text{exact}}$. These properties are illustrated in Fig. 4, where we plot E_{var} against ΔE and E_{PT2} for 10 000 randomly selected SCI internal spaces in H_2O (STO-3G). We systematically target the ground state by ensuring that the HF determinant is always included in the internal space. The linear asymptote (black dashed) and the validity of $E_{\text{PT2}} \sim \Delta E$ are clear for $E_{\text{var}} \rightarrow E_{\text{exact}}$.

III. INSIGHTS FROM A TWO-STATE MODEL

In practice, linear or quadratic extrapolation procedures only work with a limited number of points and for well-converged calculations. As illustrated in Fig. 1, the variational energy generally deviates away from linearity for larger values of E_{PT2} . The cause of these deviations can be studied using a two-state model that represents the separation of the internal and external spaces in a SCI calculation, from which the relationship between E_{var} and E_{PT2} can be analytically derived.

Our model contains individual states $|\Psi_{\mathcal{I}}\rangle$ and $|\Psi_{\mathcal{A}}\rangle$ representing wave functions in the internal and external spaces, respectively,

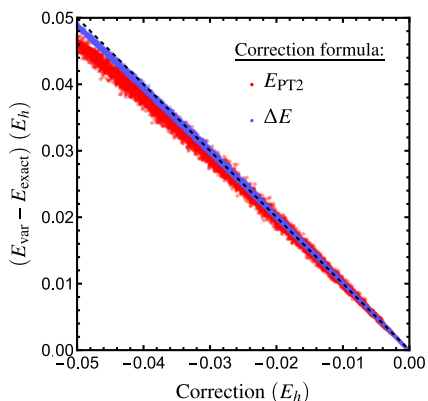


FIG. 4. Numerical illustration of the asymptotic relationships, Eqs. (12) and (15), for H₂O (STO-3G). We randomly select 10 000 sets of determinants of varying sizes (including the HF ground-state determinant) to construct the SCI internal space and variational wave function.

with characteristic energies $E_{\mathcal{I}}$ and $E_{\mathcal{A}}$. The Hamiltonian matrix in this basis is then

$$H = \begin{pmatrix} E_{\mathcal{I}} & t \\ t & E_{\mathcal{A}} \end{pmatrix}, \quad (16)$$

where $t = \langle \Psi_{\mathcal{I}} | \hat{H} | \Psi_{\mathcal{A}} \rangle$ represents the strength of the coupling between the internal and external spaces, and $\delta E = E_{\mathcal{A}} - E_{\mathcal{I}}$ provides a measure of their energetic separation. The exact ground-state energy is

$$E_{\text{exact}} = E_{\mathcal{I}} + \frac{\delta E}{2} - \sqrt{\left(\frac{\delta E}{2}\right)^2 + t^2}. \quad (17)$$

The improvement of $|\Psi_{\text{var}}\rangle$ during the course of a SCI calculation can be modeled by mixing $|\Psi_{\mathcal{I}}\rangle$ and $|\Psi_{\mathcal{A}}\rangle$ to give the parameterization,

$$|\Psi_{\text{var}}(\theta)\rangle = \cos \theta |\Psi_{\mathcal{I}}\rangle + \sin \theta |\Psi_{\mathcal{A}}\rangle, \quad (18)$$

with $0 \leq \theta < 2\pi$. The corresponding energy is

$$E_{\text{var}}(\theta) = E_{\mathcal{I}} + \frac{\delta E}{2} (1 - \cos 2\theta) + t \sin 2\theta. \quad (19)$$

Following a Taylor series expansion, the second-order correction is

$$E_{\text{PT2}}(\theta) = -\frac{1}{4} \frac{(2t \cos 2\theta + \delta E \sin 2\theta)^2}{\delta E \cos 2\theta - 2t \sin 2\theta}. \quad (20)$$

By solving Eq. (20) for θ , we can invert these equations to express E_{var} in terms of E_{PT2} as

$$E_{\text{var}} = E_{\mathcal{I}} + \frac{\delta E}{2} - E_{\text{PT2}} - \sqrt{\left(\frac{\delta E}{2}\right)^2 + t^2 + (E_{\text{PT2}})^2}, \quad (21)$$

which naturally reduces to Eq. (17) for $E_{\text{PT2}} = 0$. This expression reveals that the more general form of E_{var} as a function of E_{PT2}

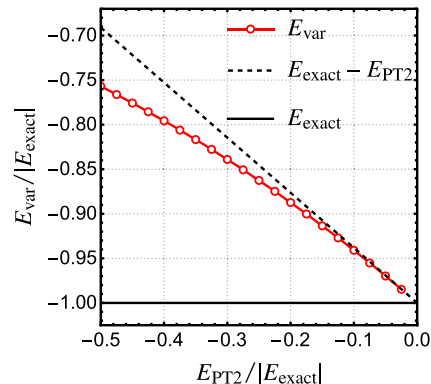


FIG. 5. E_{var} (red markers) as a function of E_{PT2} for the two-state system with $E_{\mathcal{I}} = -1$, $\delta E = 1$, and $t = 1$. These data deviate from the linear approximation (black dashed line) due to the square-root term in Eq. (21).

involves a square-root term that deviates away from linearity and that this departure from the linear regime is directly related to the energetic separation (δE) and coupling strength (t) between the internal and external spaces. For $(E_{\text{PT2}})^2 \ll \left(\frac{\delta E}{2}\right)^2 + t^2$, we recover the linear behavior $E_{\text{var}} \approx E_{\text{exact}} - E_{\text{PT2}}$. In a real SCI calculation, we expect $|t| \ll |\frac{\delta E}{2}|$. Therefore, the larger the energy separation, the sooner the linear regime is reached, while a large coupling between \mathcal{I} and \mathcal{A} also leads more rapidly to the linear regime. These features are further demonstrated through the series expansion of E_{var} at a small E_{PT2} ,

$$E_{\text{var}} = E_{\text{exact}} - E_{\text{PT2}} - \frac{E_{\text{PT2}}^2}{2\sqrt{\left(\frac{\delta E}{2}\right)^2 + t^2}} + \mathcal{O}(E_{\text{PT2}}^3), \quad (22)$$

which shows that the quadratic behavior is minimal when $|\delta E|$ or $|t|$ is large.

This functional relationship can be illustrated by evaluating E_{var} for various values of E_{PT2} in the limit of interest, as shown in Fig. 5 for $E_{\mathcal{I}} = -1$, $\delta E = 1$, and $t = 1$. As E_{PT2} gets larger, E_{var} strongly deviates from linearity and bears a close similarity to real SCI data.^{19,21,23–27,34} Figure 1 illustrates this square-root behavior for a realistic system, and the similarities between Figs. 1 and 5 are striking. For realistic systems, the two-state model can be approximately engineered using a suitable transformation of the external space \mathcal{A} such that only one external state couples to the variational wave function through the Hamiltonian, as described in Appendix B.

IV. A NON-LINEAR EXTRAPOLATION FORMULA

The insights from our two-state model suggest that a non-linear functional form may be more suitable for extrapolating SCI data. The separation of the model and perturbation space in SCI means that the relationship between E_{var} and E_{PT2} is not as straightforward as in the model system. However, as more determinants are added to the model space, the variational wave function follows a path toward the exact ground state that is likely to resemble Eq. (21). The concave form of Eq. (21) suggests that a linear extrapolation procedure will generally underestimate the exact correlation energy and

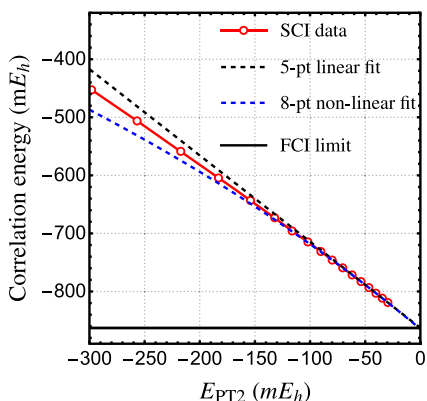


FIG. 6. Comparison of the linear and non-linear extrapolation procedures for the correlation energy of benzene computed on the cc-pVDZ basis using the SCI data from Ref. 35.

that any two-point linear fit would provide an upper bound to the exact energy. Therefore, we propose a new non-linear extrapolation formula,

$$E_{\text{var}}(E_{\text{PT2}}; a, b, c) = a + \frac{|c|}{2} - bE_{\text{PT2}} - \sqrt{\left(\frac{c}{2}\right)^2 + (bE_{\text{PT2}})^2}, \quad (23)$$

where a , b , and c are fitting parameters. This expression corresponds to a form of quadratic approximant, which has been previously used in the resummation of divergent perturbation expansions.^{60–63} Crucially, Eq. (23) reduces to a linear fit for $|E_{\text{PT2}}| \ll |\frac{c}{2b}|$ and can reproduce the observed non-linearity for larger E_{PT2} . The fitted value of a provides the estimate for the FCI result.

The variation of the FCI estimate of the correlation energy of benzene computed in the cc-pVDZ basis using a linear or non-linear extrapolation procedure is compared in Fig. 6. These data show that the non-linear formula can accurately fit the SCI data at larger E_{PT2} values than the linear procedure. In the left panel

of Fig. 7, we study the influence of the number of points included in the linear, quadratic, or non-linear fits, each of them starting from the point associated with the smallest value of E_{PT2} . The error bars indicate the standard errors associated with the fitting procedure. The fits are weighted according to the inverse square of the perturbative corrections. Although the FCI estimates obtained from the non-linear formula [see Eq. (23)] have larger fitting errors for a small number of points, they quickly stabilize and remain relatively consistent compared to those obtained from the linear procedure, which rises much faster. Consequently, a larger number of points can, and should, be employed for the non-linear extrapolation formula, while the linear extrapolation procedure becomes systematically worse when more points are used. Our results also demonstrate that, except for small numbers of points, the quadratic and non-linear fits are nearly identical. However, in contrast to the quadratic fit, the non-linear formula will never predict a maximum in E_{var} vs E_{PT2} .

In the right panel of Fig. 7, we consider a fixed-length window of consecutive points for the linear, quadratic, and non-linear fits, but we vary the index of the starting point, with the point at index 1 corresponding to the smallest value of E_{PT2} (i.e., the higher the index of the starting point, the larger the E_{PT2} correction). Using five points for the linear fit and eight points for the quadratic and non-linear fits, we again show that the quadratic and non-linear procedures are slightly more stable than the linear version with respect to the starting point, although all extrapolation schemes eventually underestimate the correlation energy for larger E_{PT2} values. These results indicate that, compared to the linear approach, the non-linear extrapolation procedure can provide a more accurate estimate of the FCI result for SCI calculations that are less well converged.

The benzene example offers a practical illustration that is close to the upper limit of what is currently achievable using SCI methods.^{19,21,35} However, since the exact FCI correlation energy remains unknown, there are potential ambiguities in the comparison of different extrapolation procedures. Instead, we turn to another example where the Hilbert space is significantly smaller, allowing the SCI calculations to be converged to the FCI limit. We consider the water molecule with the geometry used in Ref. 25, for which the exact (frozen-core) correlation energy in the cc-pVDZ

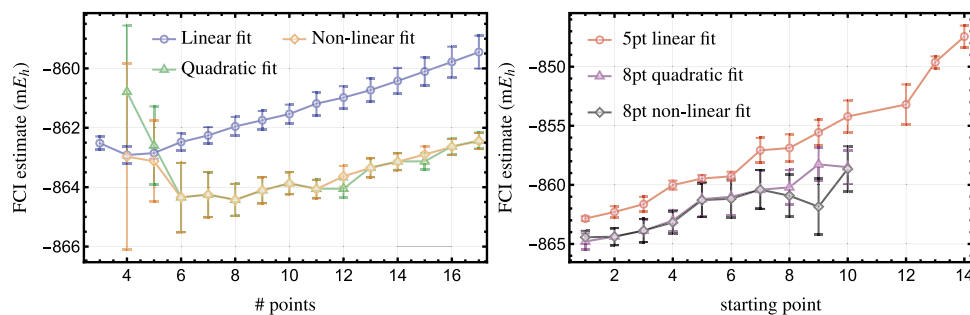


FIG. 7. Evolution of the FCI estimate of the correlation energy of benzene computed on the cc-pVDZ basis. *Left:* A variable number of fitting points is considered in the linear (blue), quadratic (green), or non-linear (orange) fits, with each fit starting from the point associated with the smallest value of E_{PT2} . *Right:* A fixed-length window of consecutive points is used for the linear (red), quadratic (purple), or non-linear (black) fits. The point of index 1 corresponds to the smallest value of E_{PT2} , and a higher index for the starting point corresponds to a larger E_{PT2} correction. The error bars indicate the standard errors associated with the fitting procedure.

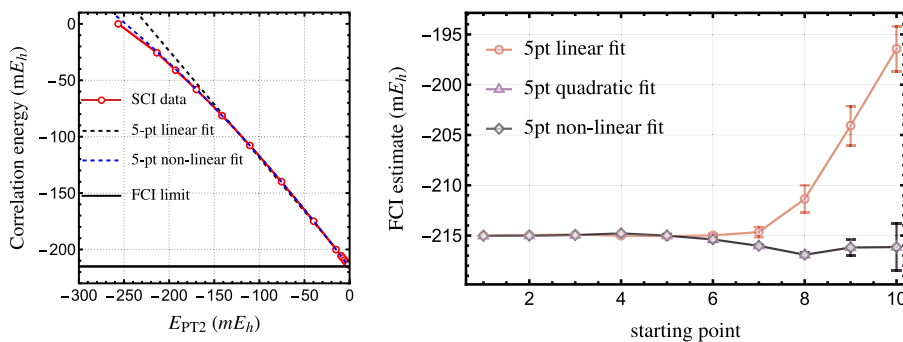


FIG. 8. Left: Comparison of the linear and non-linear extrapolation procedures for the correlation energy of water computed in the cc-pVQZ basis. The linear and non-linear weighted fits are performed with five points with minimal and maximal values of $E_{\text{PT2}} = 9.5 \times 10^{-3} E_{\text{h}}$ and $E_{\text{PT2}} = 1.1 \times 10^{-1} E_{\text{h}}$, respectively. (The quadratic fit is almost indiscernible from the non-linear fit.) Right: A five-point window of consecutive points is used for the linear (red), quadratic (purple), or non-linear (black) fits. The point of index 1 corresponds to a value of $E_{\text{PT2}} = 1.6 \times 10^{-3} E_{\text{h}}$, and a higher starting point index corresponds to a larger E_{PT2} correction. The error bars indicate the standard errors associated with the fitting procedure.

basis set is -215.027 mE_h . We conduct a ground-state CIPSI calculation based on HF orbitals. The calculation is intentionally halted prematurely to assess the feasibility of estimating the true correlation energy with smaller variational spaces. Once again, we evaluate and compare the performance of linear, quadratic, and non-linear fits.

The left panel in Fig. 8 reports the convergence of the variational correlation energy as a function of E_{PT2} as well as the five-point linear and non-linear fits obtained with minimal and maximal values of $E_{\text{PT2}} = 9.5 \times 10^{-3} E_{\text{h}}$ and $E_{\text{PT2}} = 1.1 \times 10^{-1} E_{\text{h}}$, respectively. (The quadratic fit is almost indiscernible from the non-linear fit.) The right panel in Fig. 8 shows the FCI estimates produced from the linear, quadratic, and non-linear fits relying on a five-point window of consecutive points. (The point of index 1 corresponds to a value of $E_{\text{PT2}} = 1.6 \times 10^{-3} \text{ mE}_h$.) Once again, the quadratic and non-linear fitting procedures are nearly identical and have considerably greater stability for less well-converged calculations compared to the linear version. For example, considering a set of only 351 determinants as the largest variational space (which is associated with a PT2 value of $7.5 \times 10^{-2} E_{\text{h}}$), the estimated FCI value is -216.192 mE_h , which is in error by around 1 mE_h, while the linear fit predicts -204.07 mE_h .

V. CONCLUDING REMARKS

In this article, we have proposed a theoretical rationale for the linear extrapolation procedure of the variational zeroth-order energy, E_{var} , as a function of the second-order perturbative correction, E_{PT2} , commonly employed in SCI methods. Our derivation is based on connecting the SCI variational wave function to the properties of the underlying electronic energy landscape. The accuracy of the extrapolation of E_{var} for $E_{\text{PT2}} \rightarrow 0$ is critical for accurately estimating the final FCI value.

Our investigations led us to the discovery of a novel non-linear extrapolation formula that more effectively captures the behavior of E_{var} for larger E_{PT2} values, thereby enhancing the robustness of extrapolations toward the FCI limit. Based on a two-state model, we derived the analytic form of this non-linear extrapolation formula and examined its mathematical properties. In particular, we

illustrated that the rate at which the linear regime is attained is primarily determined by the energetic gap and the coupling between the internal and external spaces. As a concrete example, we studied the ground-state correlation energy of benzene and water, which illustrates the versatility and reliability of this new extrapolation procedure.

We anticipate that our findings will provide a useful contribution to the computational toolbox for performing SCI calculations. In particular, introducing a mathematically motivated non-linear extrapolation alongside linear and quadratic approaches provides an alternative route to gain confidence in the validity of extrapolation procedures. While our numerical results indicate that the non-linear extrapolation performs similarly to a quadratic fit, the non-linear approach has the advantage that it cannot create a maximum in E_{var} vs E_{PT2} , preventing catastrophically unphysical extrapolations. Furthermore, we expect that our two-state model and our framing of the SCI approach within the electronic energy landscape framework will allow other intriguing mathematical aspects of these methods to be explored in the future.

SUPPLEMENTARY MATERIAL

See the supplementary material for the SCI data in Fig. 1 and the raw data associated with Figs. 7 and 8.

ACKNOWLEDGMENTS

H.G.A.B. acknowledges Downing College, Cambridge, for financial support through the Kim and Julianna Silverman Research Fellowship. P.-F.L. acknowledges the financial support from the European Research Council (ERC) under the European Union's Horizon 2020 research and innovation program (Grant Agreement No. 863481).

AUTHOR DECLARATIONS

Conflict of Interest

The authors have no conflicts to disclose.

Author Contributions

Hugh G. A. Burton: Conceptualization (equal); Formal analysis (equal); Investigation (equal); Writing – original draft (equal).
Pierre-François Loos: Conceptualization (equal); Formal analysis (equal); Investigation (equal); Writing – original draft (equal).

DATA AVAILABILITY

The data that support the findings of this study are available within the article and its supplementary material.

APPENDIX A: DERIVATION OF THE EPSTEIN–NESBET CORRECTION

The formal connections between internal and external spaces can be understood through the structure of the Hamiltonian matrix in the union space $\mathcal{I} \cup \mathcal{A}$.³³ Considering these two disjoint subspaces, the corresponding Schrödinger equation reads

$$\begin{pmatrix} \mathbf{H}_{\mathcal{I}} & \mathbf{h}^{\dagger} \\ \mathbf{h} & \mathbf{H}_{\mathcal{A}} \end{pmatrix} \cdot \begin{pmatrix} \mathbf{c}_{\mathcal{I}} \\ \mathbf{c}_{\mathcal{A}} \end{pmatrix} = E \begin{pmatrix} \mathbf{c}_{\mathcal{I}} \\ \mathbf{c}_{\mathcal{A}} \end{pmatrix}, \quad (\text{A1})$$

where

$$\mathbf{H}_{\mathcal{I}} = \sum_{II' \in \mathcal{I}} |I\rangle H_{II'} \langle I'|, \quad (\text{A2a})$$

$$\mathbf{H}_{\mathcal{A}} = \sum_{\alpha\alpha' \in \mathcal{A}} |\alpha\rangle H_{\alpha\alpha'} \langle \alpha'| \quad (\text{A2b})$$

are the Hamiltonian blocks associated with the internal and external spaces, respectively, and \mathbf{h} is the corresponding coupling block with elements $\langle \alpha | \hat{H} | I \rangle$. Using the Löwdin partitioning technique,⁶⁴ the second row of Eq. (A1) yields

$$\mathbf{c}_{\mathcal{A}} = (E\mathbf{1} - \mathbf{H}_{\mathcal{A}})^{-1} \cdot \mathbf{h} \cdot \mathbf{c}_{\mathcal{I}}, \quad (\text{A3})$$

while, from the first row, one gets

$$\mathbf{H}_{\mathcal{I}} \cdot \mathbf{c}_{\mathcal{I}} + \mathbf{h}^{\dagger} \cdot \mathbf{c}_{\mathcal{A}} = E\mathbf{c}_{\mathcal{I}}. \quad (\text{A4})$$

Substituting Eq. (A3) into Eq. (A4) leads to the non-linear Schrödinger equation,

$$\mathbf{H}_{\mathcal{I}}^{\text{eff}}(E) \cdot \mathbf{c}_{\mathcal{I}} = E\mathbf{c}_{\mathcal{I}}, \quad (\text{A5})$$

where the energy-dependent effective Hamiltonian reads⁶⁵

$$\mathbf{H}_{\mathcal{I}}^{\text{eff}}(E) = \mathbf{H}_{\mathcal{I}} + \mathbf{h}^{\dagger} \cdot (E\mathbf{1} - \mathbf{H}_{\mathcal{A}})^{-1} \cdot \mathbf{h}. \quad (\text{A6})$$

Solving this non-linear eigensystem is hard and unpractical due, mainly, to its energy dependence and the inversion of a large matrix. Therefore, one usually relies on educated approximations by (i) setting $E \approx E_{\mathcal{I}} = \mathbf{c}_{\mathcal{I}}^{\dagger} \cdot \mathbf{H}_{\mathcal{I}} \cdot \mathbf{c}_{\mathcal{I}}$ in the right-hand side of Eq. (A6) in order to wash away the energy dependence, hence the non-linearity; and (ii) enforcing a diagonal approximation for $\mathbf{H}_{\mathcal{A}}$, that is,

$$\mathbf{H}_{\mathcal{A}} \approx \sum_{\alpha \in \mathcal{A}} |\alpha\rangle H_{\alpha\alpha} \langle \alpha|. \quad (\text{A7})$$

One then ends up with an approximate energy expression,

$$E \approx E_{\mathcal{I}} + \sum_{\alpha \in \mathcal{A}} \frac{|\langle \alpha | \hat{H} | I \rangle|^2}{E_{\mathcal{I}} - H_{\alpha\alpha}}, \quad (\text{A8})$$

which is equivalent to the second-order Epstein–Nesbet perturbation correction in Eq. (2).

APPENDIX B: CONNECTING THE TWO-STATE MODEL TO REALISTIC SYSTEMS

For realistic systems, the two-state model can be approximately engineered using a singular value decomposition (SVD) of the gradient vector. Since the relevant components of the gradient [see Eq. (7)] form a $N_{\mathcal{A}} \times 1$ vector (where $N_{\mathcal{A}}$ is the number of external states), an SVD can be used to transform the external space \mathcal{A} such that only one direction has a non-zero gradient, meaning that only one state $|\Psi_{\mathcal{I}}\rangle = \sum_{\alpha \in \mathcal{A}} c_{\alpha} |\alpha\rangle$ couples to the variational wave function $|\Psi_{\mathcal{I}}\rangle$ through the Hamiltonian. Under this transformation, we obtain $E_{\mathcal{I}} = \langle \Psi_{\mathcal{I}} | \hat{H} | \Psi_{\mathcal{I}} \rangle$, $t = \langle \Psi_{\mathcal{A}} | \hat{H} | \Psi_{\mathcal{I}} \rangle$, and $E_{\mathcal{A}} = \langle \Psi_{\mathcal{A}} | \hat{H} | \Psi_{\mathcal{A}} \rangle$, where remaining indirect Hamiltonian coupling terms are ignored. This process can be illustrated for a Hamiltonian with two states in both the internal and external spaces, giving

$$\mathbf{H} = \begin{pmatrix} H_{00} & 0 & H_{0\alpha} & H_{0\beta} \\ 0 & H_{11} & H_{1\alpha} & H_{1\beta} \\ H_{\alpha 0} & H_{\alpha 1} & H_{\alpha\alpha} & H_{\alpha\beta} \\ H_{\beta 0} & H_{\beta 1} & H_{\beta\alpha} & H_{\beta\beta} \end{pmatrix}. \quad (\text{B1})$$

The $H_{\alpha 0} = \langle \alpha | \hat{H} | 0 \rangle$ elements directly couple the internal and external spaces and are proportional to the relevant gradient components $g_{\alpha} = 2H_{\alpha 0}$. The SVD ensures that $|0\rangle$ directly couples to only one external state, giving

$$\mathbf{H} = \begin{pmatrix} H_{00} & 0 & H_{1\alpha'} & 0 \\ 0 & H_{11} & H_{1\alpha'} & H_{1\beta'} \\ H_{\alpha' 0} & H_{\alpha' 1} & H_{\alpha'\alpha'} & H_{\alpha'\beta'} \\ 0 & H_{\beta' 1} & H_{\beta'\alpha'} & H_{\beta'\beta'} \end{pmatrix}. \quad (\text{B2})$$

Ignoring the indirect coupling elements $H_{\alpha' 1}$ and $H_{\alpha'\beta'}$ then gives the two-state model with $E_{\mathcal{I}} = H_{00}$, $t = H_{\alpha' 0}$, and $E_{\mathcal{A}} = H_{\alpha'\alpha'}$. Furthermore, since the states within \mathcal{I} are decoupled by solving the CI problem, we can construct this two-state model for any variational state by choosing $|\Psi_{\mathcal{I}}\rangle$ and performing the SVD on the corresponding gradient vector. Therefore, this two-state model can represent both ground and low-lying excited states using different values of $E_{\mathcal{I}}$, δE , and t . While this transformation is not feasible in practice, it conceptually links real SCI data and the present two-state model.

REFERENCES

- C. F. Bender and E. R. Davidson, *Phys. Rev.* **183**, 23 (1969).
- J. L. Whitten and M. Hackmeyer, *J. Chem. Phys.* **51**, 5584 (1969).
- B. Huron, J. P. Malrieu, and P. Rancurel, *J. Chem. Phys.* **58**, 5745 (1973).
- R. J. Buenker and S. D. Peyerimhoff, *Theor. Chim. Acta* **35**, 33 (1974).

- ⁵S. R. White, *Phys. Rev. Lett.* **69**, 2863 (1992).
- ⁶S. R. White, *Phys. Rev. B* **48**, 10345 (1993).
- ⁷G. K.-L. Chan and S. Sharma, *Annu. Rev. Phys. Chem.* **62**, 465 (2011).
- ⁸J. J. Eriksen, F. Lipparini, and J. Gauss, *J. Phys. Chem. Lett.* **8**, 4633 (2017).
- ⁹J. J. Eriksen and J. Gauss, *J. Chem. Theory Comput.* **14**, 5180 (2018).
- ¹⁰J. J. Eriksen and J. Gauss, *J. Chem. Theory Comput.* **15**, 4873 (2019).
- ¹¹J. J. Eriksen and J. Gauss, *J. Phys. Chem. Lett.* **10**, 7910 (2019).
- ¹²M. Motta and S. Zhang, *Wiley Interdiscip. Rev.: Comput. Mol. Sci.* **8**, e1364 (2018).
- ¹³J. Lee, F. D. Malone, and D. R. Reichman, *J. Chem. Phys.* **153**, 126101 (2020).
- ¹⁴E. Xu, M. Uejima, and S. L. Ten-no, *Phys. Rev. Lett.* **121**, 113001 (2018).
- ¹⁵E. Xu, M. Uejima, and S. L. Ten-no, *J. Phys. Chem. Lett.* **11**, 9775 (2020).
- ¹⁶I. Magoulas, K. Gururangan, P. Piecuch, J. E. Deustua, and J. Shen, *J. Chem. Theory Comput.* **17**, 4006 (2021).
- ¹⁷G. Karthik, D. J. Emiliano, S. Jun, and P. Piotr, *J. Chem. Phys.* **155**, 174114 (2021).
- ¹⁸P.-F. Loos, A. Scemama, and D. Jacquemin, *J. Phys. Chem. Lett.* **11**, 2374 (2020).
- ¹⁹J. J. Eriksen, T. A. Anderson, J. E. Deustua, K. Ghanem, D. Hait, M. R. Hoffmann, S. Lee, D. S. Levine, I. Magoulas, J. Shen, N. M. Tubman, K. B. Whaley, E. Xu, Y. Yao, N. Zhang, A. Alavi, G. K.-L. Chan, M. Head-Gordon, W. Liu, P. Piecuch, S. Sharma, S. L. Ten-no, C. J. Umrigar, and J. Gauss, *J. Phys. Chem. Lett.* **11**, 8922 (2020).
- ²⁰J. J. Eriksen, *J. Phys. Chem. Lett.* **12**, 418 (2021).
- ²¹P.-F. Loos, Y. Damour, and A. Scemama, *J. Chem. Phys.* **153**, 176101 (2020).
- ²²M. Caffarel, T. Applencourt, E. Giner, and A. Scemama, *J. Chem. Phys.* **144**, 151103 (2016).
- ²³A. A. Holmes, C. J. Umrigar, and S. Sharma, *J. Chem. Phys.* **147**, 164111 (2017).
- ²⁴A. D. Chien, A. A. Holmes, M. Otten, C. J. Umrigar, S. Sharma, and P. M. Zimmerman, *J. Phys. Chem. A* **122**, 2714 (2018).
- ²⁵P.-F. Loos, A. Scemama, A. Blondel, Y. Garniron, M. Caffarel, and D. Jacquemin, *J. Chem. Theory Comput.* **14**, 4360 (2018).
- ²⁶P.-F. Loos, M. Boggio-Pasqua, A. Scemama, M. Caffarel, and D. Jacquemin, *J. Chem. Theory Comput.* **15**, 1939 (2019).
- ²⁷P. F. Loos, F. Lipparini, M. Boggio-Pasqua, A. Scemama, and D. Jacquemin, *J. Chem. Theory Comput.* **16**, 1711 (2020).
- ²⁸M. Vérité, A. Scemama, M. Caffarel, F. Lipparini, M. Boggio-Pasqua, D. Jacquemin, and P.-F. Loos, *Wiley Interdiscip. Rev.: Comput. Mol. Sci.* **11**, e1517 (2021).
- ²⁹E. Giner, A. Scemama, and M. Caffarel, *Can. J. Chem.* **91**, 879 (2013).
- ³⁰E. Giner, A. Scemama, and M. Caffarel, *J. Chem. Phys.* **142**, 044115 (2015).
- ³¹M. Caffarel, T. Applencourt, E. Giner, and A. Scemama, "Using CLPSI nodes in diffusion Monte Carlo," in *Recent Progress in Quantum Monte Carlo* (ACS, 2016), Chap. 2, Vol. 1234, pp. 15–46.
- ³²Y. Garniron, A. Scemama, P.-F. Loos, and M. Caffarel, *J. Chem. Phys.* **147**, 034101 (2017).
- ³³Y. Garniron, A. Scemama, E. Giner, M. Caffarel, and P. F. Loos, *J. Chem. Phys.* **149**, 064103 (2018).
- ³⁴Y. Garniron, T. Applencourt, K. Gasperich, A. Benali, A. Ferté, J. Paquier, B. Pradines, R. Assaraf, P. Reinhardt, J. Toulouse, P. Barbaresco, N. Renon, G. David, J. P. Malrieu, M. Vérité, M. Caffarel, P. F. Loos, E. Giner, and A. Scemama, *J. Chem. Theory Comput.* **15**, 3591 (2019).
- ³⁵Y. Damour, M. Vérité, F. Koskoski, M. Caffarel, D. Jacquemin, A. Scemama, and P.-F. Loos, *J. Chem. Phys.* **155**, 134104 (2021).
- ³⁶Y. Damour, R. Quintero-Monsebaiz, M. Caffarel, D. Jacquemin, F. Koskoski, A. Scemama, and P.-F. Loos, *J. Chem. Theory Comput.* **19**, 221 (2023).
- ³⁷J. B. Schriber and F. A. Evangelista, *J. Chem. Phys.* **144**, 161106 (2016).
- ³⁸N. M. Tubman, J. Lee, T. Y. Takeshita, M. Head-Gordon, and K. B. Whaley, *J. Chem. Phys.* **145**, 044112 (2016).
- ³⁹N. M. Tubman, D. S. Levine, D. Hait, M. Head-Gordon, and K. B. Whaley, *arXiv:1808.02049* (2018).
- ⁴⁰N. M. Tubman, C. D. Freeman, D. S. Levine, D. Hait, M. Head-Gordon, and K. B. Whaley, *J. Chem. Theory Comput.* **16**, 2139 (2020).
- ⁴¹A. A. Holmes, N. M. Tubman, and C. J. Umrigar, *J. Chem. Theory Comput.* **12**, 3674 (2016).
- ⁴²S. Sharma, A. A. Holmes, G. Jeanmairet, A. Alavi, and C. J. Umrigar, *J. Chem. Theory Comput.* **13**, 1595 (2017).
- ⁴³Y. Yao, E. Giner, J. Li, J. Toulouse, and C. J. Umrigar, *J. Chem. Phys.* **153**, 124117 (2020).
- ⁴⁴Y. Yao and C. J. Umrigar, *J. Chem. Theory Comput.* **17**, 4183 (2021).
- ⁴⁵H. R. Larsson, H. Zhai, C. J. Umrigar, and G. K.-L. Chan, *J. Am. Chem. Soc.* **144**, 15932 (2022).
- ⁴⁶X. Liu and J. E. Subotnik, *J. Chem. Theory Comput.* **10**, 1004 (2014).
- ⁴⁷W. Liu and M. R. Hoffmann, *J. Chem. Theory Comput.* **12**, 1169 (2016).
- ⁴⁸Y. Lei, W. Liu, and M. R. Hoffmann, *Mol. Phys.* **115**, 2696 (2017).
- ⁴⁹N. Zhang, W. Liu, and M. R. Hoffmann, *J. Chem. Theory Comput.* **16**, 2296 (2020).
- ⁵⁰N. Zhang, W. Liu, and M. R. Hoffmann, *J. Chem. Theory Comput.* **17**, 949 (2021).
- ⁵¹J. P. Coe, *J. Chem. Theory Comput.* **14**, 5739 (2018).
- ⁵²J. P. Coe, A. Moreno Carrascosa, M. Simmermacher, A. Kirrander, and M. J. Paterson, *J. Chem. Theory Comput.* **18**, 6690 (2022).
- ⁵³G. H. Booth, A. J. W. Thom, and A. Alavi, *J. Chem. Phys.* **131**, 054106 (2009).
- ⁵⁴D. Cleland, G. H. Booth, and A. Alavi, *J. Chem. Phys.* **132**, 041103 (2010).
- ⁵⁵N. S. Blunt, S. D. Smart, G. H. Booth, and A. Alavi, *J. Chem. Phys.* **143**, 134117 (2015).
- ⁵⁶K. Ghanem, A. Y. Lozovoi, and A. Alavi, *J. Chem. Phys.* **151**, 224108 (2019).
- ⁵⁷J. E. Deustua, J. Shen, and P. Piecuch, *Phys. Rev. Lett.* **119**, 223003 (2017).
- ⁵⁸J. E. Deustua, I. Magoulas, J. Shen, and P. Piecuch, *J. Chem. Phys.* **149**, 151101 (2018).
- ⁵⁹H. G. A. Burton, *J. Chem. Theory Comput.* **18**, 1512 (2022).
- ⁶⁰A. Marie, H. G. A. Burton, and P.-F. Loos, *J. Phys.: Condens. Matter* **33**, 283001 (2021).
- ⁶¹D. Z. Goodson, *Wiley Interdiscip. Rev.: Comput. Mol. Sci.* **2**, 743 (2012).
- ⁶²D. Z. Goodson, in *Mathematical Physics in Theoretical Chemistry, Developments in Physical and Theoretical Chemistry*, edited by S. Blinder and J. House (Elsevier, 2019), p. 295.
- ⁶³I. L. Mayer and B. Y. Tong, *J. Phys. C: Solid State Phys.* **18**, 3297 (1985).
- ⁶⁴P. O. Löwdin, *J. Chem. Phys.* **19**, 1396 (1951).
- ⁶⁵J. P. Malrieu, P. Durand, and J. P. Daudey, *J. Phys. A: Math. Gen.* **18**, 809 (1985).